Journal of Magnetism and Magnetic Materials 474 (2019) 207–214

Contents lists available at ScienceDirect

Journal of Magnetism and Magnetic Materials

journal homepage: www.elsevier.com/locate/jmmm

Research articles

Voltage dependent physical, dielectric and magnetic properties of electrodeposited $Co_{1-x}Mn_x$ alloy nanowires

Muhammad Awais[a,*], Naeem Ahmad[a,b], Suleman Khan[a], Affan Safeer[a], Khalid Javed[c], Imran Murtaza[a], Abdul Majid[d]

[a] Spintronics Lab, Department of Physics, FBAS, International Islamic University, Islamabad 44000, Pakistan
[b] Beijing National Laboratory for Condensed Matter Physics, Institute of Physics, University of Chinese Academy of Sciences, (UCAS), Beijing 100190, China
[c] Department of Physics, FC College University, Lahore, Pakistan
[d] Department of Physics, University of Gujrat, Gujrat, Pakistan

A B S T R A C T

The $Co_{1-x}Mn_x$ ($9.1 \leq x \leq 15.2$) alloy nanowires with uniform size and high density have been prepared by AC electrodeposition method into the anodized aluminum oxide AAO templates by using the different AC potential from 9 V to 13 V. A systematic study has been done about the voltage dependent physical, dielectric and magnetic properties of CoMn nanowires. The diameter and length of nanowires is found to be 95 nm and 15 μm respectively by getting the image from Secondary Electron Microscope. The Energy Dispersive X-ray Spectroscopy gave the information which shows that the composition of Mn and Co increases and decreases respectively with the increase of deposition voltage. It was observed from X-ray Diffraction data of all samples that CoMn alloy nanowires have the cubic structure and crystallite size vary from ~39.6 nm to ~48.9 nm. The Fourier Transform Infrared Spectroscopy pattern shows the presence of other materials such as CoO, MnO, and Al_2O_3 at different wavenumber range. The dielectric constant, dielectric loss, tangent loss and AC conductivity have been measured from LCR meter data at room temperature. The aforementioned dielectric properties decrease with the increase of deposition voltage due to incorporation of Mn ions and deduction of Co ions. The descending trend of AC conductivity against the increasing voltage is also due to the increase of grain boundary volume. The M-H loops of CoMn nanowires have been measured by using the Vibrating Sample Magnetometer and show the anisotropic and ferromagnetic behavior. From hysteresis loops, it is also found that magnetization reversal has nucleation mode and squareness decreases with increase of angle. The effective anisotropy is found to be along the nanowires. This study is useful to modify the physical, structural, dielectric and magnetic properties of the metallic materials according to desire devices.

1. Introduction

Nanostructure materials have fascinating and tremendous scientific and technological attention because of their numerous beneficial properties such as high strength, high surface to volume ratio, low mass density and enriched thermal, electrical, catalytic and optical behavior. Applications of metallic elements with nanostructure morphology include sensors, capacitors, magnetic storage media, batteries, water purification devices and light weight structures [1,2]. The size dependent reactivity and enriched surface area of nanostructure metallic components also make them a promising and interesting area of study for the numerous applications. Over the last decade, devotions have been paid to change the physical performance of zero-dimensional (0D), one-dimensional (1D), and two-dimensional (2D) nanostructure materials due to the numerous range of applications in the field of microelectronic devices, optical coatings, data storage media, wear resistant coatings, flat panel displays, biological implants, sensor devices, photovoltaic cells, photodiodes, photodetectors and many more [3–9]. Furthermore in the field of biomedicine magnetic nanomaterials have implementation to prevent, diagnose and treatment of a wide range of diseases at molecular and cellular scale [10]. Comparison to other techniques of nanostructure growth such as electroplating, ball milling and sputtering, template based techniques have been considered to versatile approach of different nanostructure materials under the control environment at low cost [11–15]. Template base techniques have the advantage to deposit the metals with spatial separation and consist of two steps: fabrication of the porous matrix and filling of porous matrix with necessary materials. The most common approaches are anodizing, ion-track technology, track membrane and lithography to fabricate the nano porous templates on the base of polymer film, silicon, as well as different oxide materials such as SiO_2, TiO_2, and Al_2O_3 [16–19]. Among all aforesaid template's fabrication techniques, the anodization is an efficient and feasible technique to fabricate the metal oxide nanostructure layer on the surface of metal [20]. Anodizing technique has the unique characteristic to fabricate the AAO templates. It is low cost, easy approach, highly controllable process and gives the well-organized and regular arrangement of the templates. Now a days, among the all kind of nanostructured materials, cylindrical magnetic

* Corresponding author.
E-mail address: awais.msphy334@iiu.edu.pk (M. Awais).

https://doi.org/10.1016/j.jmmm.2018.10.122
Received 13 April 2018; Received in revised form 19 October 2018; Accepted 25 October 2018
Available online 26 October 2018
0304-8853/

nanowires fabricated by controlled electrodeposition method constitute excellent strategic candidate to next generation data storage devices and engineering magnetic domain configuration [21,22]. Nanostructure of magnetic materials especially the ferromagnetic materials have the much importance in the different fields. Fundamental interest in ferromagnetic nanostructures (nanoparticles, nanowires, nanotubes, thin film) lies in appearance of incredible magnetic and transport properties as the dimensions proceed toward the length scale of few nanometer to few ten nanometer [23]. Nanostructure ferromagnetic materials, such as nickel (Ni), cobalt (Co) and iron (Fe) have been focused on research due to unique and wide range of magnetic properties [24]. Nanowires of ferromagnetic materials within single magnetic domain size exhibit an extraordinarily enhanced coercivity and high remanence ratio. These magnetic changes at nanoscale make the magnetic materials for the use of magnetic recording media and high sensitive GMR [25,26]. Different chemical composition of alloys corresponds to different crystal structure and crystallite size which results the different physical, dielectric and magnetic properties [27,28]. The understanding of such relation is very useful to investigate the different physical, electrical and magnetic properties for desired applications. The Mn based alloys have great interest because of their use in magnetic recording media industry among the 3d transition element [29–31]. The very interesting physical, chemical, structural and magnetic properties are obtained when Co and Mn makes the alloy with each other [32–34]. The combination of Co and Mn with different composition gives the different physical, dielectric and magnetic properties and helps us to understand the physics behind such properties [35].

Most of the study and research about the properties, characteristics and application of ferromagnetic materials have been investigated on three dimensional materials, thin film and nanoparticles. Some research also done on $Co_{1-x}Mn_x$ (x = 10) nanowires [36]. The variation in the morphology, structural geometry and composition of material with the help of different AC deposition potential has the significant effect to alter the physical, electrical and magnetic properties of the materials. To best of our awareness, it was the first time to fabricate $Co_{1-x}Mn_x$ nanowires with the help of electrodeposition method at different AC deposition potential and the effect of different AC deposition potential on physical, electrical and magnetic properties have been studied in detail.

2. Experimental setup

The CoMn nanowires were fabricated by AC electrodeposition method in AAO templates [37–40]. The recipe for the solution to fabricate the CoMn nanowires was prepared by using the $CoSO_4{\cdot}7H_2O$ (0.1 M), $MnSO_4{\cdot}H_2O$ (0.1 M) in 100 ml distilled water. A small amount of boric acid H_3BO_3 was also added as a homogenizing agent to enhance the deposition rate and avoid from the hydroxide formation [41]. The CoMn nanowires were fabricated at 9, 10, 11, 12 and 13 AC voltage by keeping all other parameters constant for example temperature and pH of the solution. The Al foil between the templates was used as an electrode while other electrode was of the cupper. Nanowires growth start from the bottom of AAO tubes. First metal ions M^{n+} reduce on the surface of aluminum and then metal atoms nucleate and fabricate on the surface of aluminum [42]. The growth mechanism for electrodeposited materials is given by the reaction;

$$IA + SS \rightarrow FA - SS$$

The growth mechanism is governed by the interaction energy between initial atoms and substrate surface (E_{IA-SS}) and interaction energy between initial atoms and film atoms (E_{IA-FA}). When (E_{IA-SS}) is greater than (E_{IA-FA}), the deposition occurs by the Stranski-Krastanov mechanism. When (E_{IA-SS}) is less than (E_{IA-FA}), the deposition occurs by Volmer-Weber mechanism [43]. Nanowires cannot be seen without removing the AAO templates. So AAO templates were removed by putting the samples in the solution of 0.025 M NaOH for two hours at 60 °C.

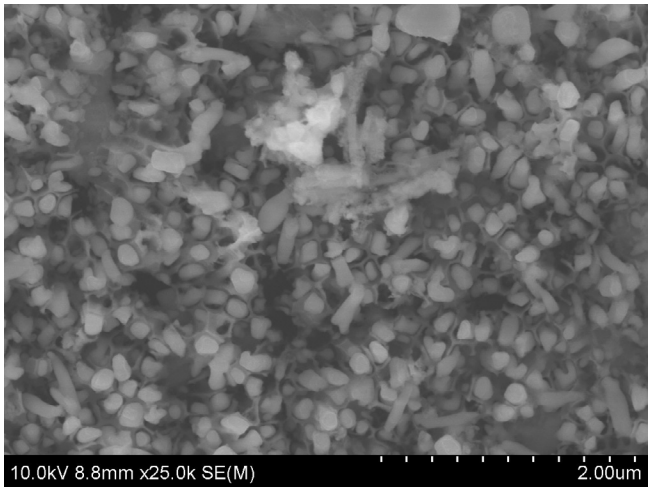

Fig. 1. SEM Image of CoMn Nanowires.

To study the surface morphology and composition of the samples, SEM and EDX (6490 LA) was used. X-ray diffractometer of wavelength CuKα (λ = 1.5405 Å) was used to investigate the phase and crystal structure of CoMn nanowires. FTIR Spectroscopy was used to investigate the existence of unknown materials and bonding between them. LCR meter (Volnic U1300 LCR meter) was used to inspect the dielectric properties of the specimen. The magnetic properties were investigated by the VSM (Lakeshore VSM) at room temperature.

3. Results and discussions

3.1. Morphological Investigation

The morphology and size of nanostructure materials is characterized by the SEM. Fig. 1 is the SEM images of the sample prepared at 11 V. According to SEM image the morphology of the sample is found to be nanowires and the diameter of nanowires is almost from 90 nm to 100 nm. The length of nanowires is 15 μm.

3.2. Composition Investigation

The composition was analyzed by EDX Spectroscopy. Fig. 2 (a) shows the EDX spectrum and composition of the sample.

As from Fig. 2 (a) oxygen, aluminum, silicon, phosphorous, manganese and cobalt are present in the sample. The first four are due to substrate and impurities but we have concern with cobalt and manganese because both are the deposited materials which make the nanowires. Fig. 2 (b) is graphical representation of Co and Mn atomic and weight percentage against the voltage. The graph shows the decreasing trend of cobalt content and increasing trend of manganese content. This effect of different percentage variation is due to the reduction potential of Co^{2+} and Mn^{2+} ions. The standard reduction potential of $Co^{2+} + 2e \rightarrow Co$ and $Mn^{2+} + 2e \rightarrow Mn$ are −0.28 V and −1.18 V respectively with respect to standard hydrogen electrode, which means Co has higher standard electrode potential than Mn. The elements at higher slandered electrode potential are suppressed at higher deposition potential [44,45]. The applied potential determine the reduction rate of Co^{2+} and Mn^{2+}. Increase of deposition potential causes the better condition for reduction of Mn^{2+} than Co^{2+}. So the rate of Mn deposition occurs high at more negative potentials (higher deposition potential) than the rate of Co deposition, which results the increase of Mn content percentage and decrease of Co content percentage in nanowires.

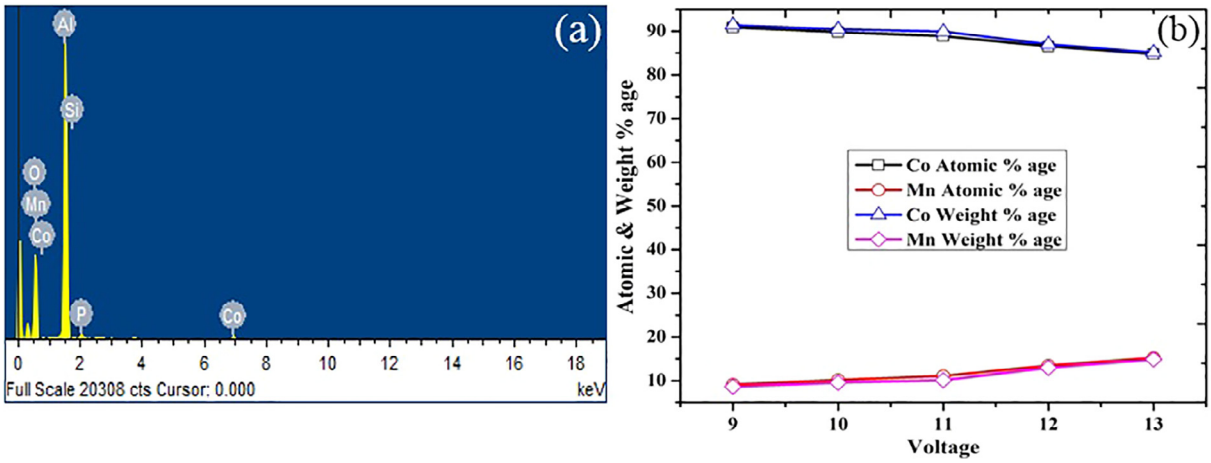

Fig. 2. (a) EDX Spectrum of CoMn Nanowires (b) Composition Variation Due to Potential.

3.3. Structural analysis

The XRD pattern of synthesized CoMn nanowires by electrodeposition method at different voltage (9, 10, 11, 12 and 13) are shown in Fig. 3 (a). The range of angle 2θ is from 10° to 80°. In all five samples the presence of very sharp peak illustrates a perfect crystal. The relative intensity of different samples has a small variation in it. This small variation in the intensity of different samples is may be due to number of reasons. These reasons include variation of the density of nanostructure on substrate, phase concentration, effect of the instrument, crystalline size and orientation of sample etc. CoMn XRD pattern has three diffraction peaks and are detected at 2θ = 44.92°, 65.41° and 78.55°. The peaks at 44.92° and 65.41° refer to cubic crystal structure of CoMn (ICSD IDs 187981) [46] with miller indices (1 1 0) and (2 0 0) respectively while the peaks at 78.55 refer to Al FCC structure (ICSD IDs 53774) with miller indices (3 1 1) [47]. The Interplanar spacing is calculated by Bragg's law and has the value of 2 Å for (1 1 0) peak and 1.4 Å for (2 0 0) peak. The unit cell parameter is 2.8 Å, Volume is 23.1 $Å^3$ and the radius is 1.4 Å.

Harris formula was used to investigate the texture coefficient;

$$TC\ (hkl) = \frac{I(hkl)/I_o(kkl)}{\frac{1}{n}\sum I(hkl)/I_o(kkl)} \quad (1)$$

Where, $I(hkl)$ is experimentally measured relative intensity, $I_o(hkl)$ is the stander relative intensity according to the JCPDS or ICSD database, and n is the number of planes or total number of reflections. The calculated data are summarized in Table 1. The values of texture coefficient that exceeded unity refer to the preferred orientation of crystallites in the corresponding planes. The acquired values of texture coefficient confirm that the (1 1 0) direction is dominant in the structure of CoMn nanowires. These values also show that with the increase of deposition voltage, the degree of texturing of nanowires increases. This indicates the increasing number of grain along the planes [48,49].

Table 1
Values of Texturing Coefficient.

2θ°	(hkl)	TC (hkl)				
		9 V	10 V	11 V	12 V	13 V
44.92	(1 1 0)	1.4725	1.4953	1.5032	1.5238	1.5369
78.55	(2 0 0)	0.5274	0.5047	0.4968	0.4761	0.4631

Debye Scherer formula was used to calculate the crystallite size of most intense peak CoMn (1 1 0) for all samples.

$$D = k\lambda/\beta\cos\theta \quad (2)$$

Where K is the shape constant and has the value of 0.9, λ represent the wavelength value of X-rays which is 1.54 Å and β is the value of full width at half maximum. Fig. 3 (b) shows that the crystallite size is increasing with the increase of voltage. The primary reasons of increasing

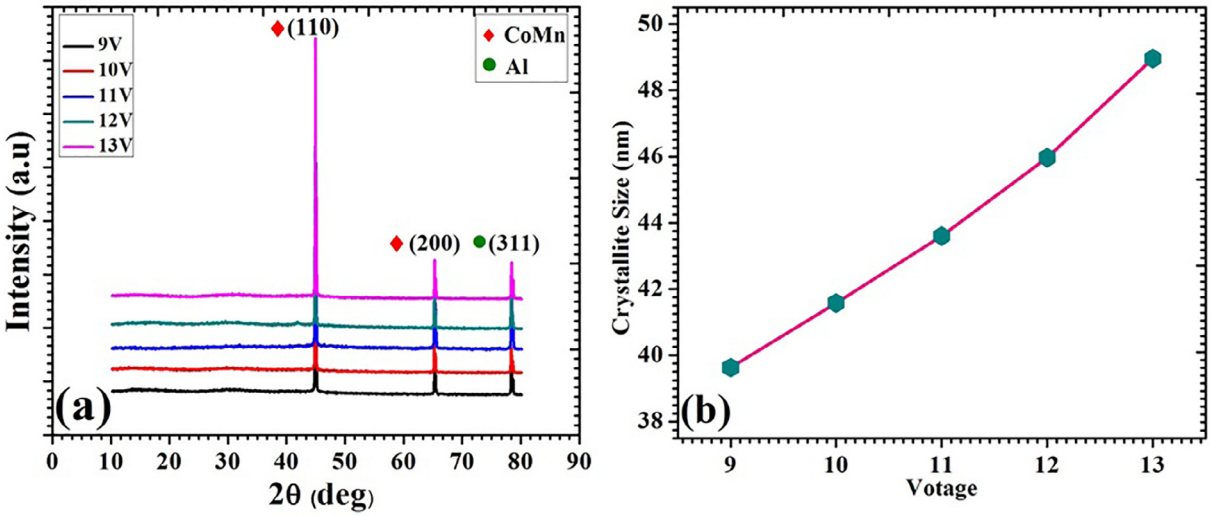

Fig. 3. (a) XRD Pattern of CoMn Nanowires (b) Crystallite Size at different Voltage.

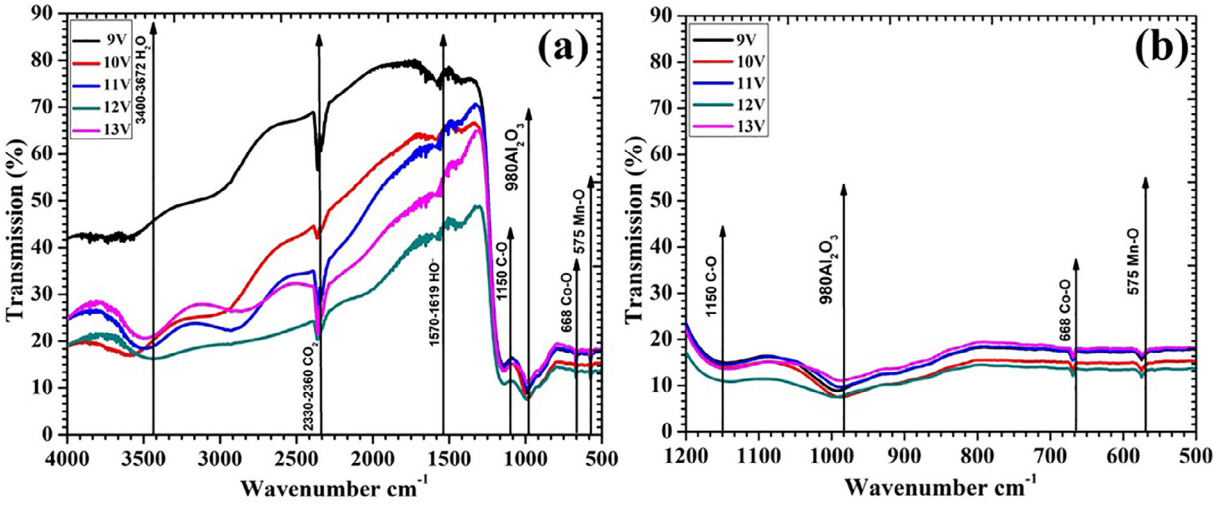

Fig 4. FTIR Spectra of CoMn Nanowires (a) Spectra from 500 cm^{-1} to 4000 cm^{-1} Wavenumber (b) Spectra from 500 cm^{-1} 1200 cm^{-1} Wavenumber.

the crystallite size is the increasing value of the texturing coefficient with the increase of deposition voltage, which leads to grow the more grains along the plane. When the deposition potential increases, crystallites stretch along the nanowire axis due to increase in growth rate [50]. The other reasons may be the agglomeration or the addition of Mn and reduction of Co composition in nanowires. The Mn and Co has the atomic radius of 204 pm and 200 pm respectively. The Mn atomic radius is greater than the Co. So increasing trend of Mn and decreasing trend of Co results the increase of crystallite size.

3.4. Fourier transform infrared spectroscopy

FTIR was used to detect the molecular bonding and identification of unknown materials in samples. In FTIR spectroscopy when IR radiations fall on a specimen, some of IR radiations are transmitted and some of them are absorbed. As a result a spectrum is obtained which is a molecular fingerprint and determine the molecular absorption and transmission. Fig. 4 shows the IR spectra of CoMn nanowires prepared in AAO templates on the aluminum substrate. The spectra were taken from wavenumber range 500 cm^{-1} to 4000 cm^{-1} as shown in Fig. 4 (a) while Fig. 4 (b) is the zoomed image of Fig. 4 (a) from wavelength range 500 cm^{-1} to 1200 cm^{-1}.

The Band observed at 575 cm^{-1} represents the bending mode of vibration of manganese oxide. The wavenumber around the 668 cm^{-1} is corresponded to vibrational bending mode of Cobalt oxide bonding [51]. The Al_2O_3 is observed at 980 cm^{-1}. The stretching bond between carbon and oxygen exists at wavenumber of 1150 cm^{-1}. The peak ranging from 1570 cm^{-1} to 1619 cm^{-1} is corresponded for hydroxyl (OH) group [52]. The peaks ranging from 2330 cm^{-1} to 2360 cm^{-1} are assigned for carbon dioxide. The stretching vibrational band in H_2O is observed at the range of 3400 cm^{-1} to 3672 cm^{-1}.

3.5. Dielectric results

LCR meter was used to study the dielectric properties of $Co_{1-x}Mn_x$ nanowires deposited on the aluminum substrate. The LCR meter gave the results of capacitance and D-factor under the frequency range of 100 Hz to 5 MHz. The values of dielectric constant were calculated with the help of the relation;

$$\varepsilon' = \frac{Cd}{\varepsilon_o A} \tag{3}$$

Where ε' is the dielectric constant or the real part of dielectrics, C is the capacitance value in farad, d is the thickness of sample in meter, ε_o is permittivity of free space and A is the area of surface cross-section. Fig. 5 (a) shows the dielectric constant graph as a function of log of frequencies. The dielectric constant reduces as the applied frequency increases and becomes constant at higher frequencies. This is ordinary because of fact that any class of species contributing to polarizability is found to show lagging behind the applied field at higher and higher frequencies. The values of dielectric constant also decreases with the increase of the voltage as shown in inset graph of Fig. 5 (a). This decrease with the voltage is due to incorporation of Mn ions and deduction of Co ions with the increase of voltage. Basically dielectric term is special for insulators. Co and Mn both are metals and have extremely low dielectric constant. Mn has more metallic character than Co. increasing Mn and decreasing Co contents results the increasing trend of metallic character. So the dielectric constant decreases. The inset graph is plotted between the maximum value of dielectric constant at initial frequency and voltage.

The dielectric loss factor ε'', which is the imaginary part of dielectrics was also calculated with the help of the relation;

$$\varepsilon'' = \varepsilon' \times \tan(\delta) \tag{4}$$

Where ε'' is the dielectric loss or imaginary part of dielectrics, ε' is the dielectric constant or the real part of the dielectrics and tan (δ) is the tangent loss or dissipation factor (D-factor) used to calculate the dielectric loss. Fig. 5 (b) shows the graph of dielectric loss as a function of log of frequencies. The dielectric loss decreases with increase of applied frequency. The values become constant at higher frequencies. The reduction of dielectric loss due to increase of frequency is attributed to decline in polarization of the specimen because the dipole cannot follow up the field variation. The dielectric loss also decreases with increase of voltage. The inset graph of Fig. 5 (b) is between the maximum values of dielectric loss at initial frequency and voltage.

Fig. 5 (c) is the graphical representation between tangent loss and log of frequencies. The values of dielectric tangent loss also decrease with the increase of frequencies. The decrease in tangent loss with the increase of frequencies may be attributed to Maxwell-Wagner polarization. The decrease in tangent loss with the increase of voltage is may be due to incorporation of Mn ions and deduction of Co ions into the lattice.

The AC conductivity is calculated by using the relation;

$$\sigma_{ac} = 2\pi f \varepsilon_o \varepsilon' \tan(\delta) \tag{5}$$

Where f is the applied frequency, ε_o is the permittivity of free space, ε' is the dielectric constant and tan (δ) is the tangent loss or dissipation factor (D-factor). Fig. 5 (d) is the illustration of AC Conductivity as a function of log of frequencies. The graph shows that at low frequencies the value of AC Conductivity is small and constant, and at higher

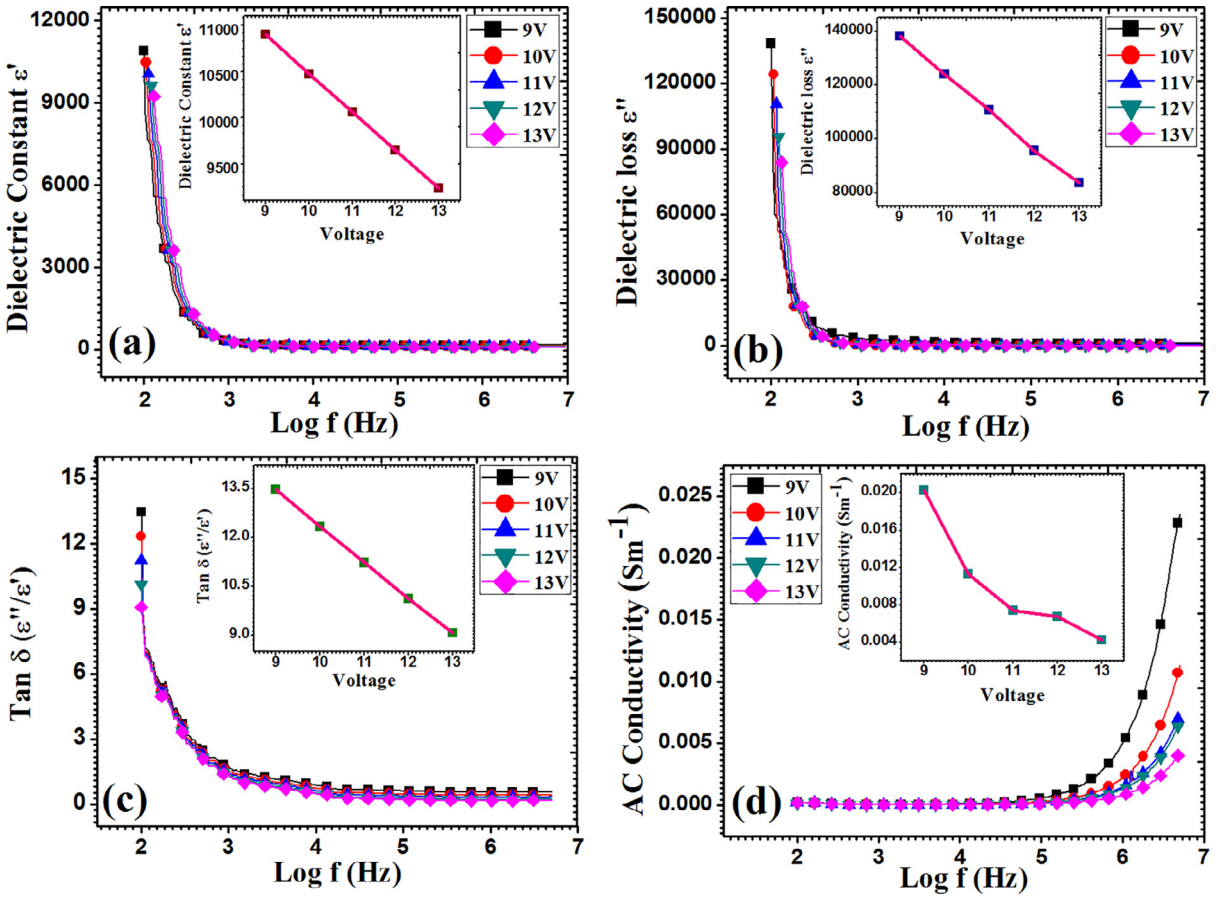

Fig. 5. (a) Dielectric Constant (b) Dielectric loss (c) Tangent loss (d) AC Conductivity as a Function of Log Frequency.

frequencies it increases suddenly and reaches its maximum value. The inset graph of Fig. 5 (d) shows that conductivity of samples is decreasing with increase of voltage. This decrease of conductivity may be due to the increasing of manganese and decreasing of cobalt composition. The AC Conductivity of cobalt and manganese is 1.7×10^7 S/m and 6.2×10^5 S/m. If composition of less conductivity material increases and composition of higher conductivity material decreases, ultimately the conductivity will decrease. The grain boundaries also affect the AC Conductivity and from XRD data the crystallite size increases with the increase of voltage so as a result grain size and the volume of the grain boundaries increases. Any increase in the volume of grain boundaries will always reduce the total value of conductivity [53]. In our case with the increase of voltage Mn composition increases and Co composition decreases. As a result grain size and grain boundaries are increases, so AC Conductivity decreases with increase of voltage.

3.6. Magnetic measurements

VSM was used to investigate the magnetic properties of the specimen which were synthesized at 9, 10, 11, 12 and 13 V.

The MH loops of all CoMn samples are shown in Fig. 6. Figure exhibits that CoMn nanowires with rich cobalt concentration shows the ferromagnetic behavior. Loops were taken at 0° and 90° and sharp difference at two angles shows the anisotropic behavior of magnetization and coercivity. The voltage dependent saturation magnetization and coercivity graph are shown in Fig. 7 (a) and (b). The value of saturation magnetization and coercivity decreases with the increase of voltage. This decreasing behavior of saturation magnetization and coercivity against the voltage is due to the addition of nonmagnetic ions and reduction of magnetic ions with the increase of voltage.

The variation of coercivity as a function of angle between nanowire axis and externally applied magnetic field is described by the magnetization reversal mechanism. The magnetization reversal mechanism is a very important phenomena in magnetic nanowires for the application of magnetic recording media. When any magnetic material is placed in externally applied magnetic field, the magnetic moments inside the materials try to align themselves in the direction of applied magnetic field. In literature, there are various possible reversal mechanism such as curling, buckling, coherent and nucleation. The coercivity as function of angle between applied magnetic field and nanowire axis provides an easy approach to define exact reversal mechanism. Fig. 7 (c) shows the reversal mechanism or angular dependence of coercivity. The curling mechanism of magnetization reversal in an infinite cylinder is define by the relation;

$$H_c = \frac{a(1+a)}{\sqrt{a^2(1+2a)Cos^2\,\theta}} H_k \tag{6}$$

Where $a = -1.08(d_c/d)^2$. This equation predicts that if the angular dependent coercivity increases with the increase of angle, it represents the curling mode of reversal mechanism [54,55]. If angular dependent coercivity decreases with the increase of angle, it shows the coherent mode of reversal mechanism and calculated by the Stoner-Wohlfarth model and is given by the formula;

$$H_n^c(\theta) = -\frac{2[K_{sh}(L_{nw}) + K_{mc}]\sqrt{1 - t^2 + t^4}}{M_o(1 + t^2)} \tag{7}$$

Where K_{sh} is shape anisotropy constant, K_{mc} is magnetocrystalline anisotropy, L_{nw} is the length of nanowire M_o is the saturation magnetization and $t = \tan(\theta)^{1/3}$, where θ is the angle between applied magnetic field and long axis of nanowires [56,57]. For coherent mode of reversal mechanism the domain wall width and coherent length should be compatible to the length or diameter of the nanowires. To obey the

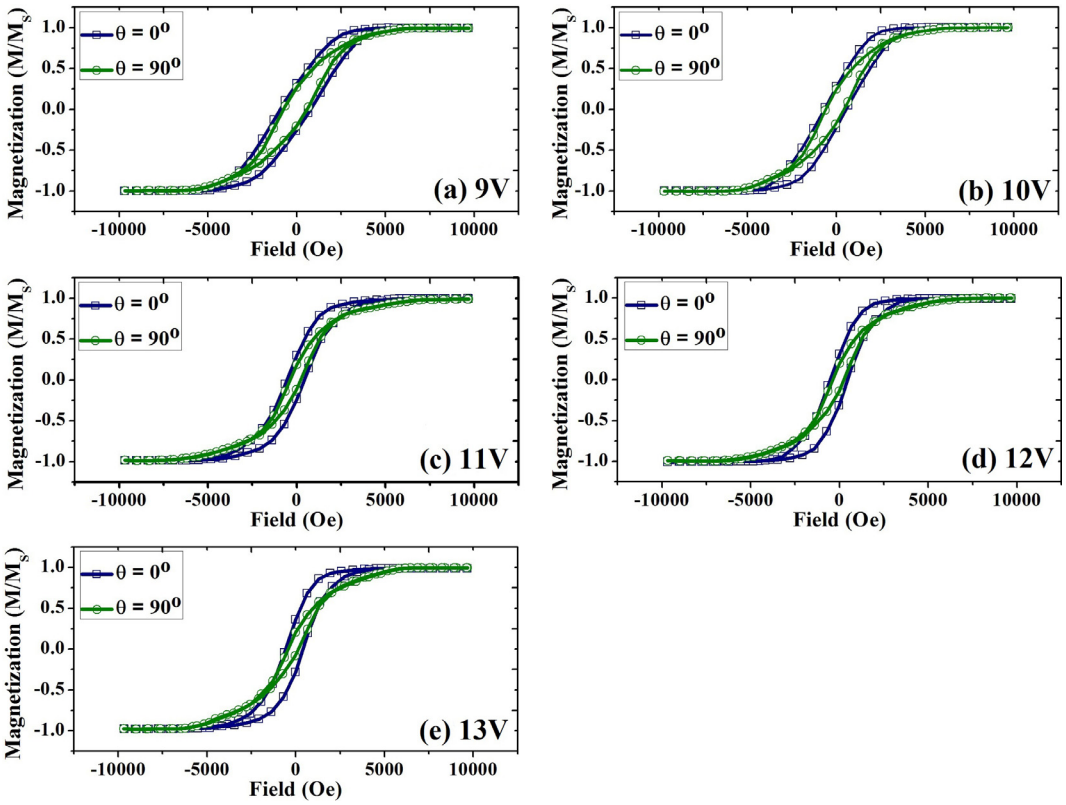

Fig. 6. M-H Curves of CoMn Nanowires.

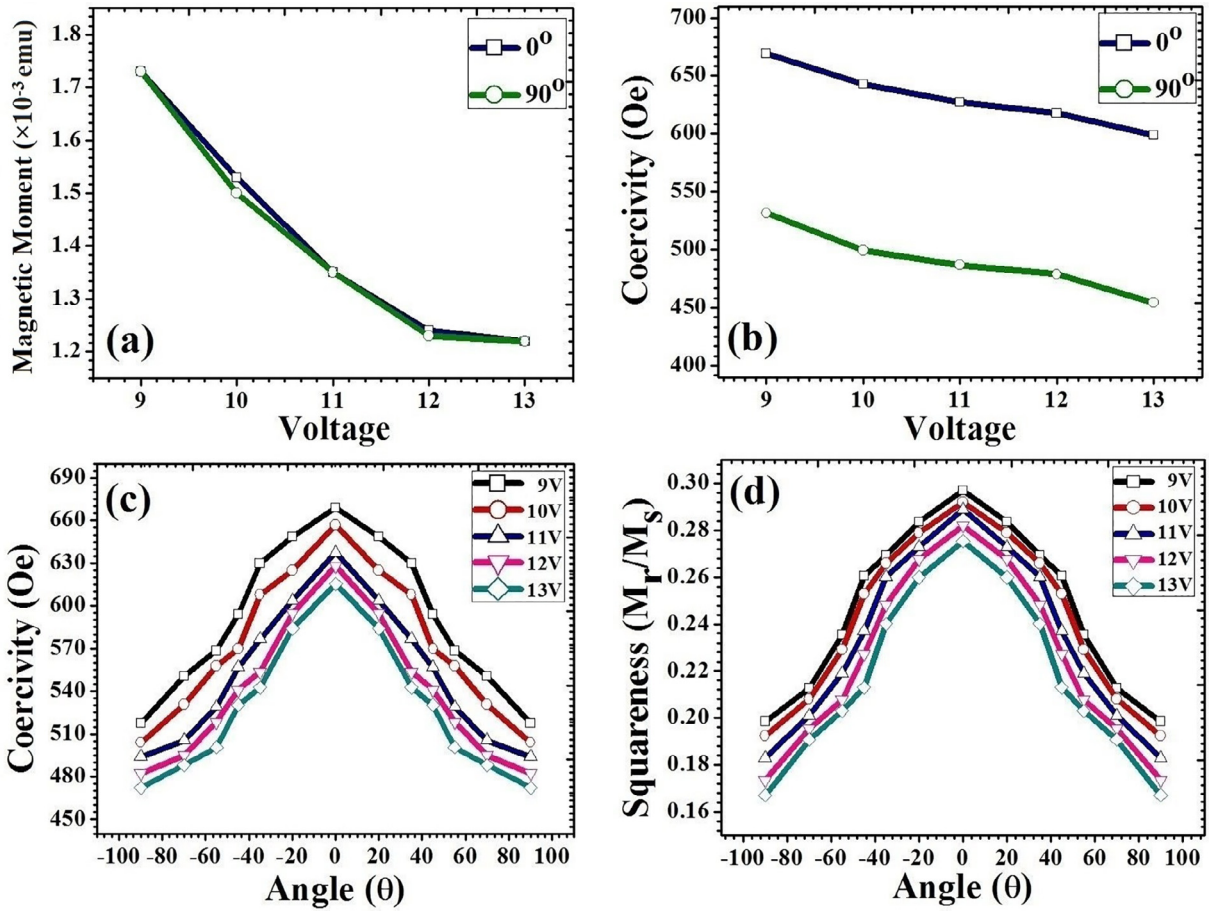

Fig. 7. (a) Magnetic Moment vs. Voltage (b) Coercivity vs. Voltage (c) Coercivity as a function of Angle (d) Squareness as a function of Angle.

value of domain wall width and coherent length the diameter and length of nanowires should be almost from 8 nm to 20 nm and from 200 nm to 500 nm respectively. From Fig. 7 (c) coercivity decreases with increase of angle and it shows the nucleation mode of magnetization reversal because the domain wall width and exchange length is not compatible to coherent length and width and exist above the critical parameter. In nucleation mode of reversal mechanism, first the domain walls nucleate at some point in nanowires and then move from one place to another.

The ratio of magnetic remanence M_r and saturation magnetization M_s shows the remanent squareness. The remanent squareness as a function of angle are shown in Fig. 7 (d). In the case of CoMn nanowires squareness in the parallel geometry is larger than that of the perpendicular geometry. The squareness is defined by effective anisotropy governed by the equation;

$$H_K = 2\pi M_S - 6.3\pi M_S r^2 L/D^3 + H_{ma} \quad (8)$$

The 1st term shows the shape anisotropy. It is the tendency which tries to align the magnetic moments along the nanowire axis (easy axis). The 2nd term is magnetostatic interaction or dipole–dipole interaction. It is the tendency which tries to align the magnetic moment perpendicular to the nanowire axis. The 3rd term shows the magneto crystalline anisotropy and it is also behave in the shape anisotropy direction but it has a negligible effect and depending upon the crystallinity of the metal. In the nanowire case the shape anisotropy is dominant so that the squareness is maximum along the easy axis, as a result the nanowires exhibit the maximum squareness along the nanowire axis (easy axis) and minimum along the perpendicular of nanowire axis (hard axis). So it shows the decreasing trend from easy axis to hard axis. Decrease in squareness results the increase of sheerness.

4. Conclusion

The $Co_{1-x}Mn_x$ ($9.1 \leq x \leq 15.2$) nanowires were fabricated at 9, 10, 11, 12 and 13 V by AC electrodeposition method in anodic aluminum oxide (AAO) templates. The SEM study illustrates that morphology of the deposited material is nanowires. The diameter and the length of the nanowires was almost 95 nm and 15 μm respectively. The EDX analysis shows that the Co and Mn composition have decreasing and increasing trend respectively with the increase of deposition voltage due to effect of reduction potential. From XRD, crystallite size of the nanowire is also increasing from ~39.6 nm to ~48.9 nm with the increase of voltage. FTIR spectra show the existence of different oxide in the samples. The dielectric study presents that dielectric constant, dielectric loss, tangent loss and AC conductivity decreases with increase of deposition voltage. The MH loops indicate the ferromagnetic and anisotropic behavior. Magnetization reversal demonstrates the nucleation mode of magnetization and squareness shows that the easy axis is along the nanowires. The angle dependent coercivity and squareness decreases with the increase of angle and shows the maximum value at 0^0 and minimum value at 90°. The net magnetic moments, coercivity, magnetization reversal and squareness decreases with the increase of deposition voltage. These variation in the structural, electrical and magnetic properties against the deposition voltage will help us to produce microelectronic devices, magnetic recording devices and high sensitive GMR. Furthermore magnetic nanomaterials with tunable properties have much importance in the field of biomedicine to transport medicine to kill the damage tissues.

Acknowledgement

Dr. Shehzad Naseem for magnetic measurements. Dr. Iftikhar Hussain gul & Ahmad Ali for dielectric measurements.

References

[1] B.C. Tappan, S.A. Steiner, E.P. Luther, Nanoporous metal foams, Angew. Chem. Int. Ed. 49 (27) (2010) 4544–4565.
[2] Matthew J. Gira, Kevin P. Takaczand, Jennifer R. Hampton, Gira, et al., Nano Convergence 3 (2016) 6.
[3] T. Thurn-Albrecht, J. Schotter, G.A. Kastle, N. Emley, T. Shibauchi, L. Krusin-Elbaum, Science 290 (2000) 2126.
[4] Wei Yang, Hu. Kai, Feng Teng, Junhui Weng, Yong Zhang, Xiaosheng Fang, Nano Lett. 18 (2018) 4697–4703.
[5] Yi Ning, Zhiming Zhang, Feng Teng, Xiaosheng Fang, Small 14 (2018) 1703754.
[6] D. Almawlawi, N. Coombs, M. Moskovite, J ApplPhys 70 (1991) 4421.
[7] S.F. Ai, G. Lu, Q. He, J.B. Li, J. Am. Chem. Soc. 125 (2003) 11140.
[8] L.W. Yin, Y. Bando, J.H. Zhan, M.S. Li, D. Golberg, Adv. Matter. 17 (2005) 1972.
[9] Y. Fukunaka, M. Motoyama, Y. Konishi, R. Ashii, Solid-State Lett. 9 (2006) c62.
[10] A.L. Kozlovskiy, I.V. Korolkov, G. Kalkabay, M.A. Ibragimova, A.D. Ibraeva, M.V. Zdorovets, V.S. Mikulich, D.V. Yakimchuk, A.E. Shumskaya, E.Yu. Kaniukov, J. Nanomater. (2017) 3060972.
[11] X.H. Li, Z. Yang, Mater. Sci. Eng. B 106 (2004) 41.
[12] F. Ebrahimi, H. Li, Scr. Mater. 55 (2006) 263.
[13] C.R. Martin, Adv. Mater. 3 (1991) 457.
[14] C.R. Martin, Chem. Mater. 81 (1996) 739.
[15] C.J. Brumlik, V.P. Menon, C.R. Martin, J. Meter. Res. 9 (1994) 1174.
[16] E. Kaniukov, D. Yakimchuk, G. Arzumanyan, H. Terryn, K. Baert, A. Kozlovskiy, M. Zdorovets, E. Belonogov, S. Demyanov, Phil. Mag. 97 (26) (2017) 2268–2283.
[17] A. Kozlovskiy, A. Zhanbotin, M. Zdorovets, I. Manakova, A. Ozernoy, T. Kiseleva, K. Kadyrzhanov, V. Rusakov, E. Kanyukov, Nucl. Instr. Meth. Phys. Res. B 381 (2016) 103–109.
[18] D. Yakimchuk, E. Kanlukov, V. Bundyulkova, L. Osminkina, S. Teichert, S. Demyanov, V. Sivakov, MRS Commun. 10 (2018) 1557.
[19] S. Demyanov, E. Kaniukov, A. Petrov, V. Sivakov, Sens. Actuators A-Phys. 216 (2014) 1–5.
[20] Weixin Ouyang, Feng Teng, Xiaosheng Fang, Adv. Funct. Mater. 28 (2018) 1707178.
[21] E. Berganza, M. Jaafar, C. Bran, J.A. Fernandez-Roldan, O. Chubykalo-Fesenko, M. Vazquez, Sci. Rep. 11 (2017) 576.
[22] Yurii P. Ivanov, Andrey Chuvilin, Sergei Lopatin, Jurgen Kosel, ACS Nano 10 (2016) 5.
[23] H. Zeng, R. Skomski, L. Menon, Y. Liu, S. Bandyopadhyay, D.J. Sellmyer, Phy. Rev. B 65 (2002) 134426.
[24] S.G. Yang, H. Zhu, D.L. Yu, Z.Q. Jin, S.L. Tang, Y.W. Du, J. Magn. Mater. 222 (2000) 97.
[25] H.P. Liang, Y.G. Guo, J.S. Hu, C.F. Zhu, L.J. Wan, C.L. Bai, InorgChem 44 (2005) 3013.
[26] A. Ramazani, M. Almasi Kashi, M. Alikhani, S. Erfanifam, J. Phy, D: Appl. Phy. 40 (2007) 5533–5536.
[27] A.E. Berkowitz, K. Takano, J. Magn. Magn. Mater. 200 (1999) 552.
[28] Naeem Ahmad, M. Suleman Khan, Arman Liaqat, Muhammad Awais, Saqlain A. Shah, Ishfaq Ahmed, Nyla Jabeen, Abdul Majid, Javed Iqbal, Appl. Phys. A 123 (2017) 65.
[29] B. Dieny, V.S. Speriosu, B.A. Gurney, S.S.P. Parkin, D.R. Whilhoit, K.P. Roche, S. Metin, D.T. Peterson, S. Nadimi, J. Magn. Magn. Mater. 93 (1991) 101.
[30] T. Sands, J.P. Harbison, M.L. Leadbeater, S. Allen, G.W. Hull Jr., R. Ramesh, V.G. Keramidas, Appl. Phys. Lett. 57 (1990) 2609.
[31] M. Tanaka, J.P. Harbison, J. Deboeck, T. Sands, B. Philips, T.L. Cheeks, V.G. Keramidas, Appl. Phys. Lett. 62 (1993) 1565.
[32] M. Tanaka, Mater. Sci. Eng. 31 (1995) 117.
[33] J. Deboeck, W. Van Roy, C. Bruynseraede, A. Van Esch, H. Bender, G. Borghs, Microelectron. J. 27 (1996) 383.
[34] M. Matsui, T. Ido, K. Sato, K. Adachi, J. Phys. Soc. Jpn. 28 (1970) 791.
[35] D. Wu, G.L. Liu, C. Jing, Y.Z. Wu, D. Loison, G.S. Dong, X.F. Jin, D.-S. Wang, Phys. Rev. B 63 (2001) 214403.
[36] Naeem Ahmad, Amna Jaral, Ghulbahar Bano, Sidrah Batool, Hira Dolpazir, Suleman Khan, Javed Iqbal, et al., J Supercond Nov Magn 29 (2016) 509–513.
[37] Dmitry L. Shimanovich, Alla I. Vorobjova, Daria I. Tishkevich, Alex V. Trukhanov, Maxim V. Zdorovets, Artem L. Kozlovskiy, J. Nanotechnol. 9 (2018) 1423–1436.
[38] Hideki Masud, Haruki Yamada, Masahiro Satoh, Hidetaka Asoh, Highly ordered nanochannel-array architecture in anodic alumina, Appl. Phys. Lett. 71 (1997) 19.
[39] Suleman Khan, Naeem Ahmad, Nisar Ahmed, Affan Safeer, Javed Iqbal, X.F.Han, Ref. MAGMA 63925, 2018.
[40] Naeem Ahmad, M. Suleman Khan, Arman Liaqat, Muhammad Awais, et al., Appl. Phys. A 123 (2017) 65.
[41] Ghafar Ali, Muhammad Maqbool, Nanoscale Res. Lett. 8 (2013) 352.
[42] Aiman Mukhtar, Babar Shehzad Khan, Tahir Mehmood, Int. J. Electrochem. Sci. 12 (2017) 4574–4584.
[43] T.I. Zubar, S.A. Sharko, D.I. Tishkevich, N.N. Kovaleva, D.A. Vinnik, S.A. Gudkova, E.L. Trukhanova, E.A. Trofimov, S.A. Chizhik, L.V. Panina, S.V. Trukhanov, A.V. Trukhanov, JALCOM 748 (2018) 970–978.
[44] Nobuaki Watanabe, Katsuhito Sano, Nsoys Tasugi, Taiki Yamaguchi, Akihiro Yamamoto, Misa Ueno, Rie Sumiyoshi, Tomiyuki Arakawa, APL Mater. 3 (2015) 041804.
[45] Jihong Duan, Xinli Kou, J. Electrochem. Soc. 160 (10) (2013) D471–D475.
[46] Persson, Kristin, Materials Data on MnCo (SG:221), ID: mp-1009133DOI 10.17188/1325581, United state September, 2016.
[47] Persson, Kristin, Materials Data on Al (SG:225), ID: mp-134, DOI 10.17188/

1189564, United state January, 2015.
[48] E.Yu Kaniukov, A.L. Kozlovsky, D.I. Shlimas, M.V. Yakimchuk, E.E. Shumskaya, K.K. Kadyrzhanov, J. Surf. Invest-X-Ray 11 (1) (2017) 270–275 ISSN 1027-4510.
[49] A.L. Kozlovsky, D.I. Shlimas, A.E. Shumskya, E.Yu Kaniukov, M.V. Yakimchuk, K.K. Kadyrzhanov, Phys. Met. Metallogr. 118 (2) (2017) 174–179 ISSN 0031-918X.
[50] E. Kaniukov, A. Kozlovsky, D. Shlimas, D. Yakimchuk, M. Zdorovets, K. Kadyrzhanov, Mater Sci Eng 110 (2016) 012013.
[51] Nisha J. Tharayil, R. Rveendran, Alexander Varghese Vaidyan, IJPAP 46 (2008) 47–56.
[52] M. Margabandhu, S. Senshilnathan, G. Vijaykumar ISSN 2351-8014, 25, pp. 1-7, 1 Jun. 2016.
[53] Michael C. Martin, Martha L. Mecartney, Solid State Ionics 161 (2003) 67–79.
[54] G.C. Han, B.Y. Zong, P. Luo, Y.H. Wu, J. Appl. Phys. AIP 93 (2003) 9202.
[55] J.Y. Naeem Ahmad, D.W. Shi Chen, Javed Iqbal, J.Xlufeng Han, Appl. Phys. 111 (2012) 07C119.
[56] Kinjal Gandha, J. Jeotikanta Mohapatra, Ping Liu, J. Magn. Magn. Mater. 04 (2017) 060.
[57] J.Y. Naeem Ahmad, Asim Husain Chen, D.W. Shi, X.F. Han, J. Magn. Magn. Mater. 378 (2015) 545–550.